Title

CRL5-dependent regulation of the small GTPases ARL4C and ARF6 controls hippocampal morphogenesis

Journal

Proceedings of the National Academy of Sciences of the United States of America, 117(37)

ISSN

0027-8424

Authors

Han, Jisoo S
Hino, Keiko
Li, Wenzhe
et al.

Publication Date

2020-09-15

DOI

10.1073/pnas.2002749117

Peer reviewed

CRL5-dependent regulation of the small GTPases ARL4C and ARF6 controls hippocampal morphogenesis

Jisoo S. Han[a,1], Keiko Hino[a,1], Wenzhe Li[a], Raenier V. Reyes[a], Cesar P. Canales[a,2], Adam M. Miltner[a], Yasmin Haddadi[a], Junqing Sun[b], Chao-Yin Chen[b], Anna La Torre[a], and Sergi Simó[a,3]

[a]Department of Cell Biology and Human Anatomy, University of California, Davis, CA 95616; and [b]Department of Pharmacology, University of California, Davis, CA 95616

Edited by Mary E. Hatten, Rockefeller University, New York, NY, and approved August 3, 2020 (received for review February 14, 2020)

The small GTPase ARL4C participates in the regulation of cell migration, cytoskeletal rearrangements, and vesicular trafficking in epithelial cells. The ARL4C signaling cascade starts by the recruitment of the ARF–GEF cytohesins to the plasma membrane, which, in turn, bind and activate the small GTPase ARF6. However, the role of ARL4C–cytohesin–ARF6 signaling during hippocampal development remains elusive. Here, we report that the E3 ubiquitin ligase Cullin 5/RBX2 (CRL5) controls the stability of ARL4C and its signaling effectors to regulate hippocampal morphogenesis. Both RBX2 knockout and Cullin 5 knockdown cause hippocampal pyramidal neuron mislocalization and development of multiple apical dendrites. We used quantitative mass spectrometry to show that ARL4C, Cytohesin-1/3, and ARF6 accumulate in the RBX2 mutant telencephalon. Furthermore, we show that depletion of ARL4C rescues the phenotypes caused by Cullin 5 knockdown, whereas depletion of CYTH1 or ARF6 exacerbates overmigration. Finally, we show that ARL4C, CYTH1, and ARF6 are necessary for the dendritic outgrowth of pyramidal neurons to the superficial strata of the hippocampus. Overall, we identified CRL5 as a key regulator of hippocampal development and uncovered ARL4C, CYTH1, and ARF6 as CRL5-regulated signaling effectors that control pyramidal neuron migration and dendritogenesis.

hippocampal development | CRL5 | ARL4C | ARF6 | pyramidal neuron migration

ARL4C is a small GTPase that belongs to the ADP-ribosylation factor (ARF)-like 4 protein subfamily (ARL4) (1, 2). Despite the high level of ARL4C (also known as ARL7) messenger RNA (mRNA) detected in human brain tissue, its function in the nervous system remains unknown (3). In epithelial cells, ARL4 proteins participate in actin cytoskeleton rearrangement, vesicle dynamics, and cell migration (1). In particular, ARL4C regulates filopodia formation, epithelial cell migration, and tubulogenesis through the regulation of the Rho GTPase family (4, 5). Molecularly, ARL4 proteins, including ARL4C, can recruit the ARF–GEF cytohesins (CYTH1–4) to the plasma membrane, which, in turn, can bind and activate the small GTPase ARF6 (5, 6). In the nervous system, ARF6 participates in dendrite and axon outgrowth and branching (7–10), apical adhesion of neural progenitors (11), and cortical neuron migration (12).

The ubiquitin–proteasome pathway plays a role in nearly every aspect of eukaryotic cell biology by targeting proteins for degradation (13). The large family of Cullin–RING E3 ligases (CRLs) are multiprotein complexes that nucleate around seven different Cullins. In particular, CRL5, the last evolved member of the family, assembles around Cullin 5 (CUL5) (14). On its C terminus, CUL5 binds the RING box 2 protein (RBX2; also known as RNF7 or SAG), a necessary step for bringing Ub~E2 to CRL5 and essential for full CRL5 activity (15). To recruit substrates for ubiquitylation, CRL5 utilizes the Elongin B/C (also known as TCEB2/TCEB1) subunits to associate with up to 38 different substrate adaptor proteins, which provide substrate specificity (15).

The core CRL5 components CUL5 and RBX2 are ubiquitously expressed during development and in the adult central nervous system (CNS) and functionally active during development (16–18). Importantly, CRL5 substrate adaptors are dynamically regulated during development, directing CRL5 activity to specific substrates at different times and areas in the CNS (19). In the neocortex, CRL5 opposes projection neuron migration by down-regulating the Reelin/DAB1 signaling pathway as migrating projection neurons reach the top of the cortical plate (18, 20, 21). In the CNS, Reelin/DAB1 signaling participates in several developmental processes, including neuron migration, dendritogenesis, axogenesis, and synaptogenesis (22–24). Moreover, CRL5 also controls levels of the tyrosine kinase FYN, which exerts important roles during development and in the adult brain (18, 25–27).

Anatomically, all mammals share a similar hippocampal substructure organization (28). The hippocampus is divided into the dentate gyrus (DG) and *cornu ammonis* (CA). The DG includes the *fascia dentata* and the hilus, and the CA is further differentiated into CA1, CA2, and CA3. Hippocampal pyramidal neurons (PNs) are born from neural progenitors in the ventricular zone (VZ) of the cortical hem and migrate to the *stratum pyramidale* (*sp*) using radial glial-aided migration (29, 30). In comparison to the neocortex, fewer signaling pathways have been identified that control neuron migration and localization in the hippocampus (29).

Here, we show that depletion of CRL5 activity disrupts localization and dendritogenesis of hippocampal PNs. We further demonstrate that this is a cell-autonomous phenotype and that

Significance

In comparison to the neocortex, the molecular mechanisms that contribute to neuron migration, particularly pyramidal neuron migration, and localization in the hippocampus remain for the most part unknown. The present study characterizes the role of the E3 ubiquitin ligase CRL5 during hippocampal pyramidal neuron migration. CRL5 down-regulates the small GTPase ARL4C and its associated signaling effectors, in a posttranscriptional fashion, to localize pyramidal neurons in the hippocampus. CRL5-dependent regulation of ARL4C signaling is also required for the formation of a single, apically oriented dendrite in pyramidal neurons and for its full outgrowth to the superficial strata of the hippocampus. Therefore, this study uncovers CRL5 and ARL4C signaling as crucial molecular determinants for hippocampal morphogenesis.

Author contributions: C.-Y.C., A.L.T., and S.S. designed research; J.S.H., K.H., W.L., R.V.R., C.P.C., A.M.M., Y.H., J.S., and S.S. performed research; J.S.H., K.H., R.V.R., A.M.M., J.S., C.-Y.C., and S.S. analyzed data; and J.S.H., A.L.T., and S.S. wrote the paper.

The authors declare no competing interest.

This article is a PNAS Direct Submission.

[1]J.S.H. and K.H. contributed equally to this work.

[2]Present address: UC Davis Center for Neurosciences and Department of Psychiatry and Behavioral Sciences, University of California, Davis, CA 95616.

[3]To whom correspondence may be addressed. Email: ssimo@ucdavis.edu.

This article contains supporting information online at https://www.pnas.org/lookup/suppl/doi:10.1073/pnas.2002749117/-/DCSupplemental.

First published September 1, 2020.

sustained Reelin/DAB1 signaling is not sufficient to cause ectopic positioning or dendritic defects in PNs. We uncover ARL4C, CYTH1/3, and ARF6 as CRL5-regulated signaling effectors and demonstrate that accumulation of ARL4C is necessary to cause the defects in PN localization and dendritogenesis observed upon CRL5 inactivation. Importantly, we also show that accumulation of ARL4C, FYN, and DAB1 are sufficient to mimic the phenotypes caused by CRL5 depletion. Furthermore, we show that ARF6 opposes PN overmigration and that a CUL5/ARF6 double knockdown exacerbates the overmigration phenotype. Finally, we show that ARL4C and ARF6 are necessary for PN dendrites to outgrow into the *stratum lacunosum moleculare* (*slm*), and, in their absence, normal apical dendrites are formed, but fail to extend past the *stratum radiatum* (*sr*). Our results support a key role for CRL5 during hippocampal morphogenesis by regulating ARL4C, FYN, and DAB1 levels and reveal an ARL4C/CYTH1/ARF6-dependent mechanism of dendritic outgrowth in PNs.

Results

Depletion of RBX2 Disrupts Projection Neuron Localization. To study the role of CRL5 in the developing hippocampus, we crossed the described *Rbx2* floxed mice (*Rbx2* fl/fl) with Emx1–Cre mice, which express Cre in the telencephalon starting at embryonic stage 9.5 (E9.5) (18, 31). In comparison to our previous reports using Nestin–Cre to deplete *Rbx2* (Rbx2cKO–Nes mice), *Rbx2* fl/fl; Emx1-Cre animals (Rbx2cKO–Emx1) were normally born, thrived as control littermates, did not show the extensive hydrocephalus phenotype present in Rbx2cKO–Nes mice, and survived until adulthood (18). As expected, efficient and extensive depletion of RBX2 was observed in Rbx2cKO–Emx1 samples at P1 when tested by Western blotting (*SI Appendix*, Fig. S1*A*). Furthermore, Rbx2cKO–Emx1 telencephalons accumulated tyrosine phosphorylated (pY)-DAB1, DAB1, and FYN and showed the same layering defects as described for Rbx2cKO–Nes pups (*SI Appendix*, Fig. S1) (16, 18). These results indicate that Rbx2cKO–Emx1 mice faithfully recapitulate the phenotypes observed in Rbx2cKO–Nes mice, without the morbidity caused by hydrocephalus.

Depletion of RBX2 cause a significant number of PNs, identified by staining against DKK3, to localized outside the *sp* when hippocampi from control and Rbx2cKO–Emx1 mice were analyzed at postnatal day 21 (P21) to P23 (Fig. 1 *A* and *B*) (32). Close examination identified ectopic PNs in the in the *stratum oriens* (*so*), which may be expected if migration is defective, but also in the *sr*/*slm*, suggesting that CRL5 regulates PN migration and opposes PN overmigration (Fig. 1 *Aa′*, *Aa″*, and *C*). Most ectopic PNs were observed in the more medial part of the CA1 region, with fewer ectopic PNs found in the CA3 (Fig. 1 *A* and *C*). The number of DKK3+ cells in the molecular layer and granule cell layer of the DG in the RBX2 mutant mice was also increased (Fig. 1 *Aa‴*, *Aa⁗*, and *C*). These results indicate that RBX2, potentially through CRL5 activity, determines the final position of PNs in the *sp* and that some PN populations, particularly those in the CA1, and DKK3+ cells in the DG, are more affected by the absence of RBX2. Similar results were observed in Rbx2cKO–Nes hippocampi, confirming the role of RBX2 in PN localization independently of the Cre driver used to deplete RBX2 (*SI Appendix*, Fig. S2).

To determine whether PN morphology was affected by RBX2 depletion, RBX2 mutant (Rbx2cKO–Nes) and control (RBX2 fl/fl) brains were stained with the Golgi–Cox impregnation method. In control samples, labeled PNs were found in the *sp* with a single, radially oriented apical dendrite extending toward the *sr*/*slm* (Fig. 1*D*, purple arrowhead). In comparison, several RBX2 mutant PNs, identified by the size of their soma and location in the *sp* and *sr*, had two main (e.g., "apical") dendrites originating at the soma and extending toward the *sr*/*slm* (Fig. 1*D*, yellow arrowheads). These results indicate that CRL5 participates in the formation of a single apical dendrite in PNs during hippocampal development.

CRL5 Regulates PN Localization in a Cell-Autonomous Fashion. Our previous studies indicated that RBX2 regulates neuron positions in the retina through cell-autonomous and non–cell-autonomous mechanisms (16). To test whether CRL5 regulates hippocampal development cell autonomously, we used in utero electroporation (IUE) to deplete CRL5 activity in individual PNs. A plasmid coexpressing a short hairpin RNA (shRNA) against CUL5 (shCUL5) and EGFP was in utero-electroporated in CD-1 embryos at E15.5, and electroporated brains were collected at P10. In comparison to controls (GFP only), depletion of CUL5 disrupted PN localization (Fig. 2). Whereas PNs expressing GFP were mostly localized in the *sp* (91.4 ± 1%) (Fig. 2 *A* and *C*), a significant amount of PNs expressing the shCUL5/GFP plasmid were found in the *sr*/*slm* (73.5 ± 0.5%) (Fig. 2 *B* and *C*). Surprisingly, few GFP+ PNs were found in the *so* when CUL5 was knocked down (KD) (0.3 ± 0.3%) (Fig. 2 *B* and *C*). Overall, these data suggest that the migration defects observed in the Rbx2cKO–Emx1 hippocampi are a combination of cell-autonomous (PN overmigration) and compensatory or non-cell-autonomous (PN migration arrest) mechanisms.

Next, we analyzed the apical dendrites in the electroporated PNs. As expected, the majority of GFP+ PNs in control electroporations showed a normal, single apical dendrite extending radially toward the *sr* and *slm* (Fig. 2*a′* and 2D). Depletion of CUL5 disrupted dendrite formation in more than 40% of the PNs analyzed (Fig. 2*b′* and 2D). Two main defects were observed: 1) a disrupted apical dendrite, where a single apical dendrite is not radially oriented toward the *sr*/*slm*; and 2) PNs with two or more "apical" dendrites (i.e., multiple apical dendrites) (Fig. 2*b′* and D). Interestingly, in the majority of cases where PNs had two "apical" dendrites, these dendrites formed a "V-shape" extending to the *sr* and the *slm*. These results are consistent with those observed in Rbx2 mutant PNs (Fig. 1*D*) and indicate that CRL5 participates in the formation of a single, radially oriented apical dendrite in hippocampal PNs.

Sustained Reelin/DAB1 Signaling Does Not Cause PN Overmigration or Dendritic Defects. CRL5 opposes Reelin/DAB1 signaling by targeting active pY-DAB1 for degradation (20). Reelin/DAB1 signaling is believed to regulate PN migration and dendrite outgrowth (33, 34). Thus, we hypothesized that sustained Reelin/DAB1 signaling might be responsible for the phenotypes observed in the Rbx2cKO mutant hippocampus. First, we confirmed that DAB1 accumulated in the Rbx2cKO–Emx1 hippocampus (Fig. 3 *A* and *B*) and in shCUL5-electroporated neurons (*SI Appendix*, Fig. S3*A*). To test whether sustained Reelin/DAB1 signaling is sufficient to promote PN overmigration, we used the *Socs7* knockout mouse (16). SOCS7 is a CRL5 substrate adaptor that recruits and targets pY-DAB1 for degradation in the developing telencephalon (18). Importantly, depletion of SOCS7 promoted an accumulation of DAB1 in the hippocampus at similar levels as in RBX2 mutant animals, but without affecting other CRL5-dependent substrates (Fig. 3 *A* and *B* and *SI Appendix*, Fig. S3*B*). Next, we analyzed the distribution of DKK3+ PNs in the SOCS7 mutant hippocampus. No differences were observed in PN position between control ($Socs7^{+/-}$) and SOCS7 mutant hippocampi (Fig. 3 *C* and *D*). Furthermore, we used IUE to express GFP in control and SOCS7 mutant PNs. The majority of GFP+ cells were found in the *sp* both in control and SOCS7 mutant hippocampi (Fig. 3*E*). Importantly, in both cases, PNs present a single, apical dendrite that extends radially to the *sr*/*slm*. These results indicate that sustained signaling from Reelin/DAB1 or from other SOCS7 targets are not sufficient to promote the PN overmigration or dendritic defects observed in the RBX2 mutant hippocampus.

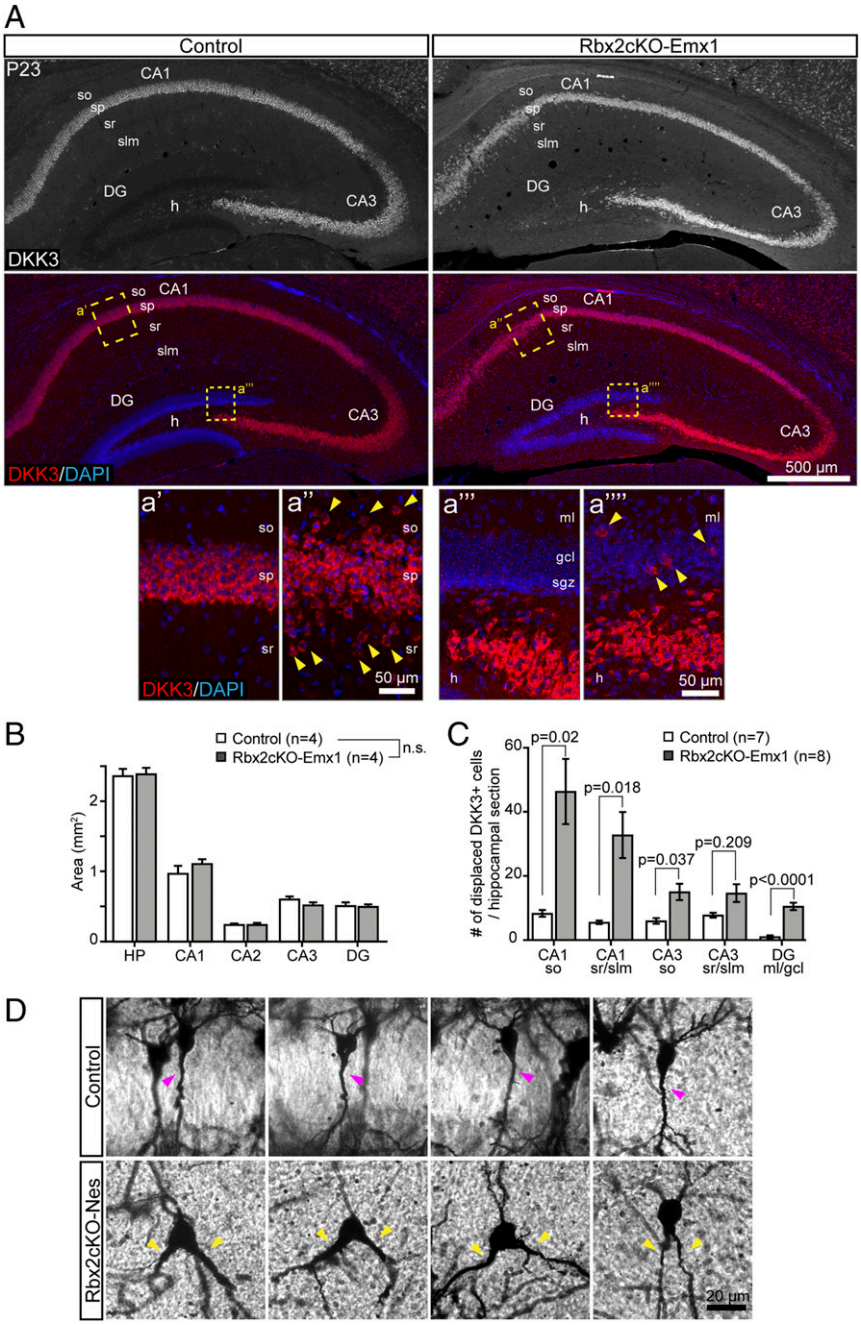

Fig. 1. RBX2 regulates PN position and apical dendrite morphology in the hippocampus. (*A*) DKK3+ PN misposition at P23. Stainings of coronal sections of Control (*Rbx2* fl/fl) and Rbx2cKO-Emx1 dorsal hippocampus against DKK3 show displaced PNs into *so*, *sr*, and *slm* in Rbx2cKO-Emx1 mice. (*a′*–*a′′′′*) High-magnification images of the CA1 (*a′* and a′) and DG (*a′′′* and *a′′′′*) showing dispersion of DKK3+ cells. Yellow arrowheads indicate displaced DKK3+ cells. (*B*) Quantification of displaced DKK3+ cells. Increased number of DKK3+ cells are observed in *so*, *sr*, and *slm* compared to wild-type littermates. Three or four sections were quantified per brain. Mean ± SEM. Statistics, multiple *t* test with Bonferroni–Dunn method adjusted *P* value. (*C*) Measurement of hippocampal areas. No differences were observed in between RBX2 fl/fl and Rbx2cKO–Emx1 samples. Mean ± SEM. Statistics, multiple *t* test with Bonferroni–Dunn method adjusted *P* value. (*D*) Abnormal multiple apical dendrites in RBX2 mutant PNs. P15 control and Rbx2cKO–Nes P15 were stained by using the Golgi silver impregnation method. "V-shaped" double apical dendrites were observed in Rbx2cKO–Nes hippocampi. Pink arrowheads indicate normal apical dendrite, and yellow arrowheads indicate double apical dendrites. gcl, granule cell layer; h, hilus; ml, molecular layer; n.s., not significant; sp, stratum pyramidale.

CRL5 Regulates Levels of ARL4C, Cytohesin-1, and ARF6 in the Developing Telencephalon. To determine which proteins and signaling pathways are responsible for the phenotypes observed in the RBX2 mutant hippocampus, we performed quantitative mass spectrometry (MS) using the tandem mass-tag (TMT) isobaric-labeling comparing control (*Rbx2* fl/fl; $n = 4$) and RBX2 mutant (Rbx2cKO–Nes; $n = 3$) P0 telencephalons (35). A total of 8,088 unique proteins with two or more peptides identified per protein were considered for further analysis (Fig. 4*A* and Dataset S1). Proteins accumulated or decreased 1.5-fold in comparison to control samples and with Student *t* test $P < 0.01$ were primarily considered as regulated by CRL5. As previously shown, levels of RBX2 and CUL5 were down-regulated and the bona fide CRL5 targets DAB1 and FYN accumulated in the RBX2 mutant samples (Fig. 4*A*) (18).

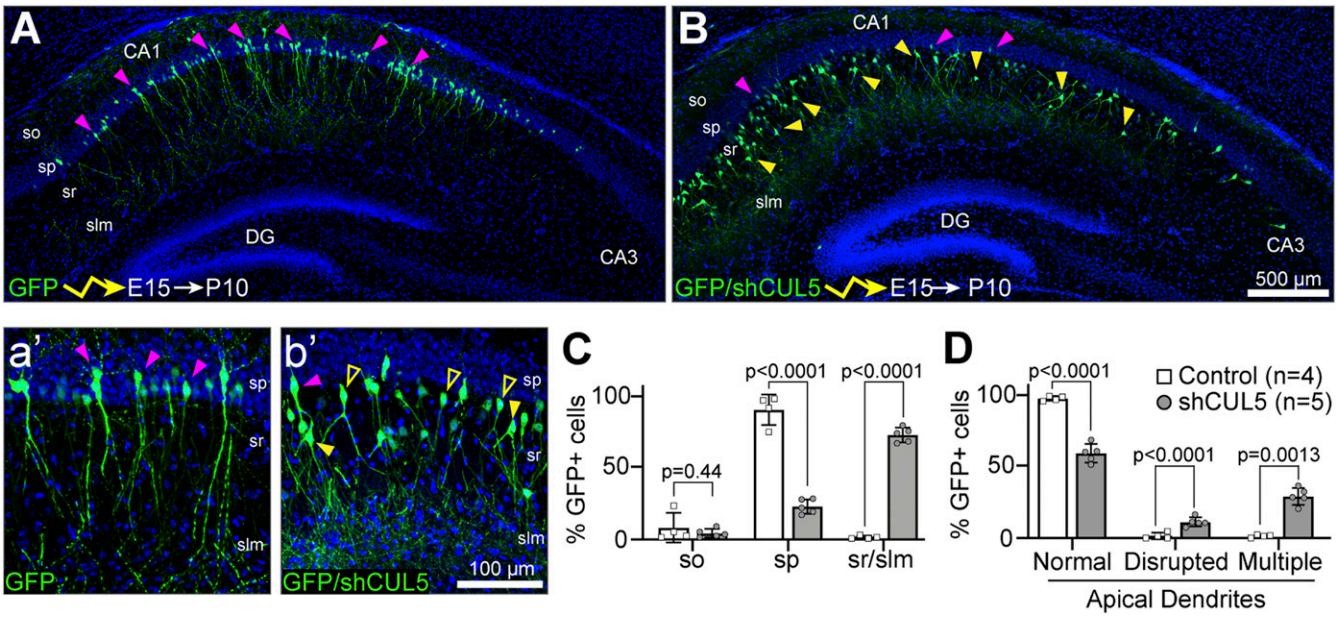

Fig. 2. CRL5 regulates PN position and apical dendrite morphology in a cell-autonomous fashion. (*A* and *B*) IUE of GFP (*A*) or GFP/shCUL5 (*B*) expressing plasmids at E15.5 embryos and samples collected at P10. shCUL5 electroporated neurons overmigrated into *sr/slm* and had V-shaped multiple apical dendrites. (*a*′ and *b*′) High-magnification images of *A* and *B* shows detailed PN morphology and dendritic formation. Pink arrowheads indicate PNs with correct position and apical dendrite. Yellow arrowheads indicate overmigrated PNs with abnormal apical dendrites. Yellow hollow arrowheads indicate overmigrated PNs with normal apical dendrite. (*C* and *D*) Quantification of the percentage number of displaced GFP+ cells/total GFP+ cells (*C*) and percentage number of GFP+ cells with normal, disrupted (single apical dendrite with abnormal orientation), and multiple (two or more) apical dendrites in electroporated hippocampal samples. At least three sections were quantified per electroporated brain. Mean ± SD. Statistics, multiple *t* test with Bonferroni–Dunn method adjusted *P* value.

The same results were observed in hippocampal samples from Rbx2cKO–Emx1 mice when levels of RBX2, pY-DAB1/DAB1, and p-SFK/FYN were analyzed by Western blotting (Fig. 4*C*). These results further confirmed that, at the molecular level, RBX2, potentially through CRL5 activity, regulates DAB1 and FYN levels independently of the Cre driver mouse used to knock out *Rbx2*. We observed the accumulation of 20 proteins in the RBX2 mutant telencephalons, including ARL4C, CYTH1/3, and ARF6 (Fig. 4*A*). Importantly, we confirmed by Western blotting that ARL4C, CYTH1, and ARF6 significantly accumulated in the hippocampus of Rbx2cKO–Emx1 mice at perinatal stages (Fig. 4*C*), suggesting that CRL5 regulates levels of ARL4C and ARL4C signaling effectors in the hippocampus. However, these results cannot determine whether CRL5-dependent regulation is a direct (e.g., recruiting, polyubiquitylating, and targeting effectors for degradation) or indirect (e.g., affecting levels of gene transcription) phenomenon. To test whether transcription was affected in RBX2 mutant mice, we compared the transcriptome of control and Rbx2cKO–Nes telencephalons at P1 by RNA sequencing (RNA-seq). Absence of RBX2 did not significantly alter the expression profile of any detected gene, including DAB1, FYN, ARL4C, CYTH1/3, or ARF6 (Fig. 4*B* and Dataset S2). These results indicate that CRL5-dependent regulation of ARL4C, CYTH1/3, and ARF6 is posttranscriptional.

To test whether accumulation of ARL4C, CYTH1, and ARF6 resulted in higher signaling pathway activation, first, we assessed CYTH1/ARF6 binding levels by coimmunoprecipitation and showed that total CYTH1/ARF6 binding is increased in the absence of RBX2 (Fig. 4*D*). Next, we examined whether increased CYTH1/ARF6 binding resulted in activation of ARF6 (i.e., ARF6–GTP) in the hippocampus. Using the ARF-binding domain from the Golgi-associated, gamma adaptin ear-containing, ARF binding protein 3 (GGA3) in pull-down assays (36), we detected significantly higher levels of ARF6–GTP in Rbx2cKO–Emx1 samples in comparison to control (Fig. 4*E*). All together, these data suggest that in absence of RBX2, accumulation of ARL4C promotes the recruitment of CYTH1, which, in turn, binds and activates ARF6. Importantly, depletion of SOCS7 does not affect levels of ARL4C, CYTH1, or ARF6 during hippocampal development (Fig. 4*F*).

ARL4C Is Dynamically Expressed during Hippocampal Development. To determine the role of ARL4C in the developing murine hippocampus, we first determined its ontogenic expression. ARL4C was expressed in the hippocampus with maximal expression between P5 and P9, which correlates with PN apical dendrite outgrowth, and minimal expression at embryonic and juvenile stages (Fig. 5 *A* and *B*). These changes in protein expression are driven by posttranscriptional mechanisms, as no significant differences in *Arl4C* mRNA levels were detected during postnatal development and in the adult hippocampus (Figs. 4*B* and 5*C*). Importantly, absence of RBX2 promotes ARL4C accumulation at any stage of development, suggesting that CRL5 is constantly regulating ARL4C levels (Fig. 5*D*). Immunofluorescence against ARL4C in a P8 mouse brain indicated that ARL4C is ubiquitously expressed in the brain (*SI Appendix*, Fig. S4). Expression of ARL4C was detected in the cytoplasm of PNs and granule cells of the DG of control and RBX2 mutant hippocampi, albeit at a higher level in the latter (Fig. 5*E* and *SI Appendix*, Fig. S4).

In hippocampal PNs, ARL4C was detected in puncta, mostly in the cytoplasm ,but also in the nucleus, and diffused at the plasma membrane (*SI Appendix*, Fig. S5*A*). To determine whether ARL4C localization was changing in response to RBX2 depletion, we cultured E17.5 hippocampal neurons from control and Rbx2cKO–Emx1 embryos and analyzed ARL4C expression at 4 d in vitro (DIV). In culture neurons from control hippocampi, ARL4C was detected in puncta in the cytoplasm, both in the soma and neurites, as well as at the plasma membrane (*SI Appendix*, Fig. S5*B*). RBX2 mutant PNs showed a similar ARL4C distribution as in the controls, but with an increased ARL4C signal both at the plasma membrane and in puncta (*SI Appendix*, Fig. S5*C*). Interestingly, depletion of RBX2 significantly increased the total number of ARL4C+ puncta in the cell (*SI Appendix*, Fig. S5*D*). These results confirm that depletion of RBX2

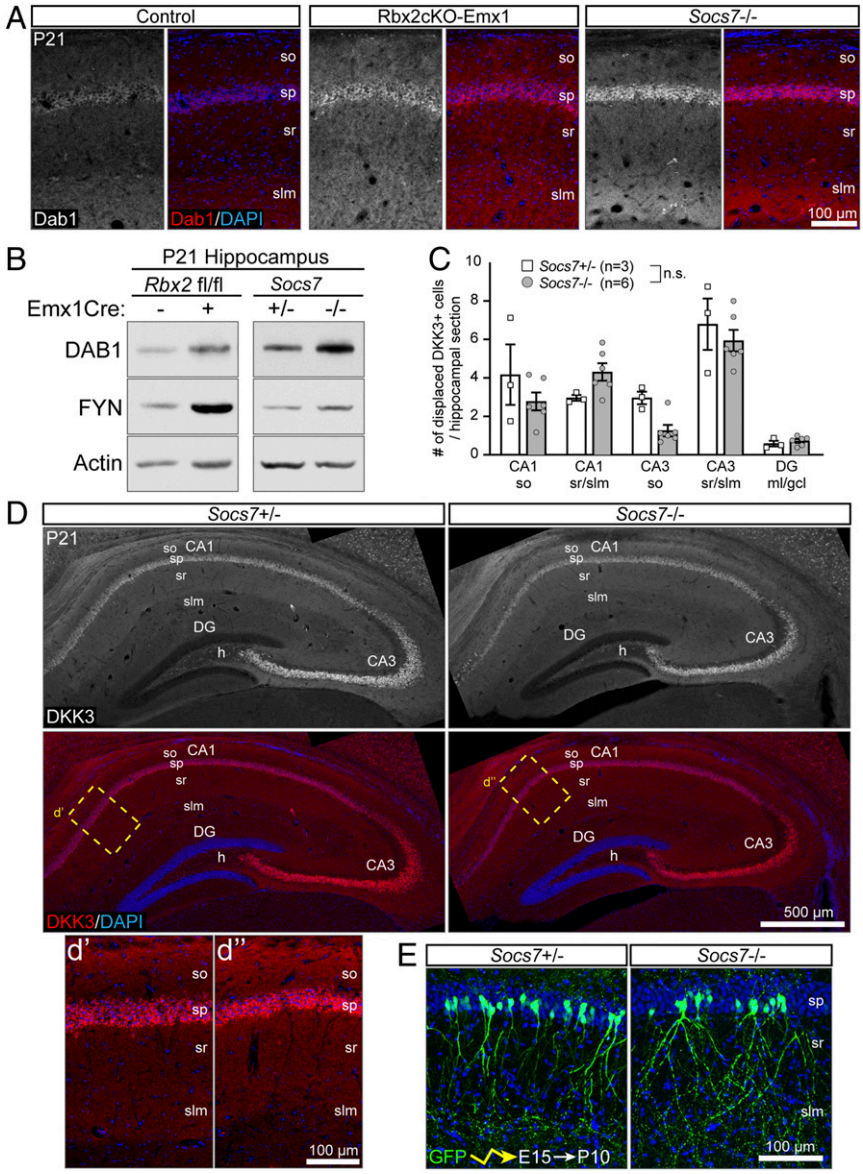

Fig. 3. DAB1 accumulation is not sufficient to disrupt PN positioning or apical dendrite morphology. (*A*) DAB1 accumulated in both Rbx2cKO–Emx1 and SOCS7$^{-/-}$ hippocampi in comparison to control (*Rbx2* fl/fl). Coronal sections of P21 hippocampi were stained with anti-DAB1 and counterstained with DAPI. (*B*) Representative images of Western blotting experiments indicating that DAB1 accumulated in both Rbx2cKO–Emx1 and SOCS7$^{-/-}$ hippocampal samples, but FYN only accumulated in Rbx2cKO–Emx1 P21 hippocampal lysates. (*C*) Quantification of displaced DKK3+ cells. No difference was observed between genotypes. At least three sections quantified per brain. Mean ± SD. Statistics, multiple *t* test with Bonferroni–Dunn method adjusted *P* value. (*D*) Coronal sections of P21 SOCS7$^{+/-}$ and SOCS7$^{-/-}$ hippocampi were stained with an anti-DKK3 antibody and counterstained with DAPI. (*d′* and *d′′*) High-magnification images of the CA1 indicating that normal PN localization in SOCS7$^{-/-}$ hippocampi. (*E*) IUE of GFP in SOCS7$^{+/-}$ and SOCS7$^{-/-}$ embryos at E15.5 and collected at P10. Electroporated GFP+ PNs show normal positioning and apical dendrites. n.s., not significant.

promotes ARL4C accumulation at the single-cell level, that ARL4C is distributed both in puncta and at the plasma membrane in hippocampal neurons, and suggest that neurons oppose the increased levels of ARL4C by storing it in intracellular vesicles.

ARL4C Participates in Dendritic Development In Vitro. Given that ARL4C expression correlates with dendrite formation and maturation in hippocampal PNs and that ARL4C regulates cytoskeleton dynamics in epithelial cell lines (4, 37), we assessed whether ARL4C participates in PN dendritogenesis. E17.5 hippocampal primary neurons were cotransfected with a hARL4C expression plasmid or a shARL4C-expressing plasmid along with an EGFP expression plasmid (Fig. 6*A*). We fixed the cells after 2 d and measured neurite complexity by Sholl analysis. In comparison to controls, overexpression of hARL4C significantly reduced neurite complexity (Fig. 6 *A* and *B*). On the contrary, depletion of endogenous ARL4C increased neurite complexity (Fig. 6 *A* and *B*). Interestingly, when the distance of the longest neurite was measured, which usually corresponds to the developing axon, no differences were observed between conditions (Fig. 6*C*), nor was the complexity of the longest neurite affected in any condition (Fig. 6*B*; >60 µm). These results suggest that ARL4C participates in the formation of the dendritic tree in hippocampal neurons without affecting the growth or complexity of the prospective axon.

ARL4C and ARF6 Regulate PN Migration and Dendrite Formation during Hippocampal Development. Finally, we tested the possibility that accumulation of ARL4C, CYTH1, and/or ARF6 in PNs

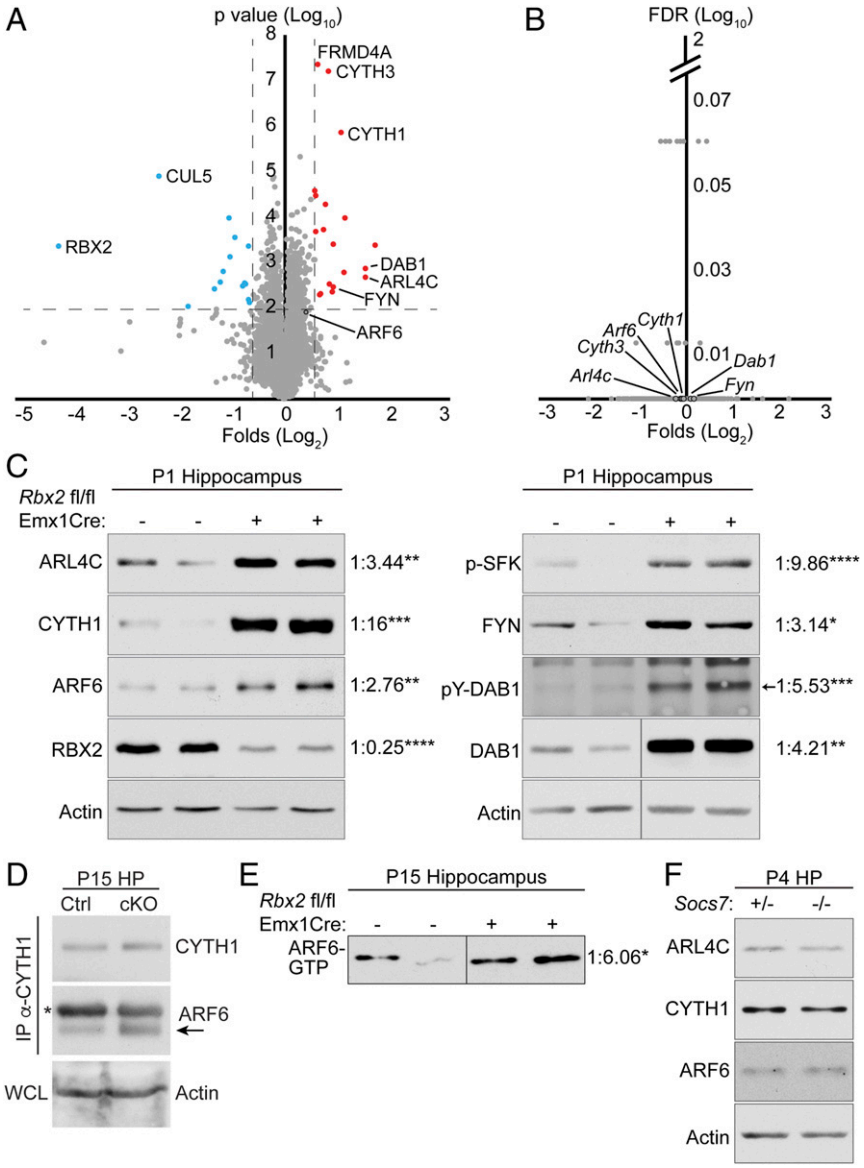

Fig. 4. ARL4C, Cytohesin-1, and ARF6 accumulate in the RBX2 mutant, but not in SOCS7$^{-/-}$ hippocampi. (*A*) TMT-MS of Rbx2cKO–Nes ($n = 3$) and *Rbx2* fl/fl ($n = 4$) telencephalons (P0) plotted as a ratio of Rbx2cKO-Nes/control. The *x* axis represents the logarithmic fold ration of Rbx2cKO–Nes/control per protein identified. The *y* axis represents the logarithmic *P* value of the *t* test per protein identified. Proteins whose differentially expression in comparison to control (*Rbx2* fl/fl) have a $P < 0.01$ and accumulated above 1.5 folds (red dots) or reduced lower than 0.666 folds (blue dots) in comparison to control were initially considered for further studies. As expected, RBX2 mutant samples showed lower levels of RBX2 and CUL5 and higher levels of DAB1 in comparison to control. (*B*) RNA-seq analysis comparing Rbx2cKO–Nes (Mutant; $n = 3$) and *Rbx2* fl/fl (Control; $n = 3$) telencephalon at P1 was performed to determine transcriptionally differences between genotypes. Ratio of counts per million between Rbx2cKO–Nes and control per gene is plotted. The *x* axis represents the logarithmic fold ration of Rbx2cKO–Nes/control per gene identified. The *y* axis represents the logarithmic false discovery rate value (FDR; or q value) calculated by using the Benjamini, Krieger, and Yekutieli method. Only genes with an average count per million (cpm) in control samples of >1 were used for statistical purposes and plotted. No significant transcriptomic differences were observed between genotypes. (*C*) Western blot analyses validating TMT-MS data in P1 Rbx2cKO–Emx1 and control hippocampi. Arrow indicates pY-DAB1 band in anti–p-Tyr blot. Numbers indicate ratio of proteins in *Rbx2* fl/fl ($n = 5$) vs. Rbx2cKO–Emx1 ($n = 3$). Statistics, Student's *t* test. $^*P < 0.05$; $^{**}P < 0.01$; $^{***}P < 0.001$; $^{****}P < 0.0001$. (*D*) Increased binding between CYTH1 and ARF6 in the Rbx2cKO-Emx1 hippocampus in comparison to control. An anti-CYTH1 antibody was used to immunoprecipitated CYTH1 and Western blotting was used to determine the levels of ARF6 coimmunoprecipitated. Representative blot of *Rbx2* fl/fl (Ctrl; $n = 4$) and Rbx2cKO–Emx1 (cKO; $n = 3$) coimmunoprecipitation is shown. Arrow indicates ARF6 band, * indicates IgG. (*E*) Elevated ARF6-GTP levels were detected in Rbx2cKO–Emx1 hippocampal lysates by using a GGA3–GST pull-down assay in comparison to control. Numbers indicate ratio of ARF6–GTP detected in *Rbx2* fl/fl ($n = 3$) vs. Rbx2cKO–Emx1 ($n = 3$). Statistics, Student's *t* test. $^*P < 0.05$. (*F*) ARL4C, CYTH1, and ARF6 did not accumulate in P4 SOCS7 $^{-/-}$ (n= 3) in comparison to controls (SOCS7 $^{+/-}$; $n = 4$) hippocampus lysates when analyzed by Western blotting. Statistics, Student's *t* test. WCL, whole-cell lysate.

was responsible for the migration and dendritic phenotypes observed upon CRL5 inactivation (Fig. 7 *A* and *B*). Using IUE, we KD CUL5 together with ARL4C, CYTH1, or ARF6 from hippocampal PNs (Fig. 7 *C*–*E*). Depletion of ARL4C completely rescued the overmigration phenotype caused by CUL5 KD, and the majority of PNs were found in the *sp* with a single apical dendrite toward the *sr* (Fig. 7 *C* and *F*). However, the dendritic tree of CUL5/ARL4C-KD PNs failed to extend into the *slm*. Apical dendrites from CUL5/ARL4C-KD PNs emerged normally, but an obvious increase in dendritic arborization occurred at the lower end of the *sr* and did not extend into the *slm* (Fig. 7*C*).

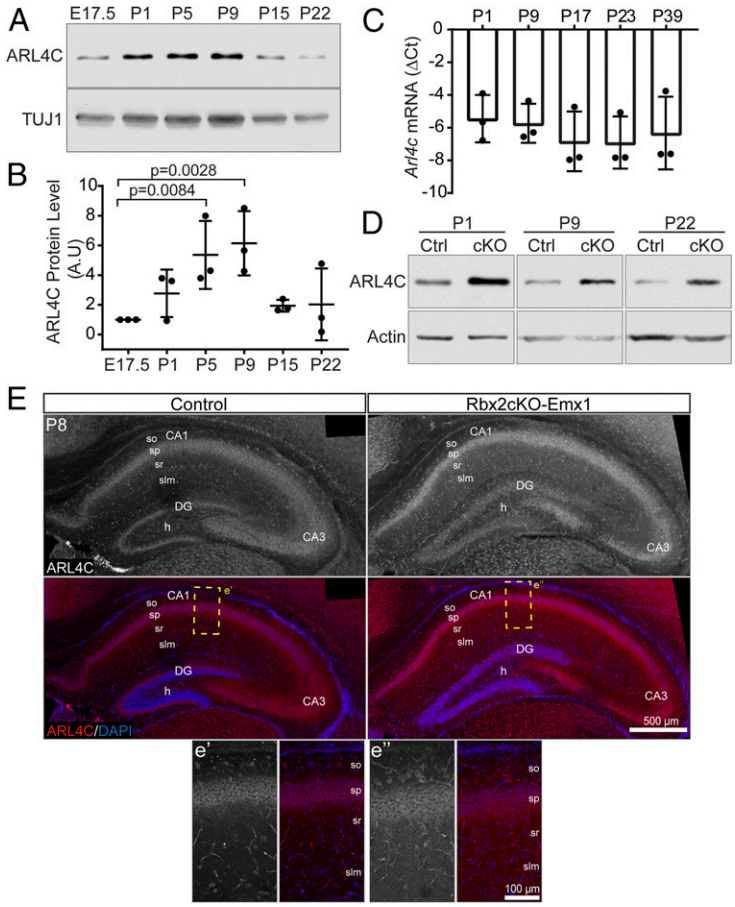

Fig. 5. ARL4C is dynamically expressed during hippocampal development. (*A*) Ontogenic analysis of ARL4C expression in the hippocampus during development by Western blotting. (*B*) Quantification of ARL4C Western blots in *A* and normalized to ARL4C expression at E17.5. Mean ± SD. Statistics, one-way ANOVA. A.U., arbitrary units. (*C*) No changes were observed in *Arl4c* transcript levels between ages P1 to P39 by qPCR analysis. Cycle differences between *Arl4c* and *β-Actin* from three independent experiments are plotted. Mean ± SD. Statistics, one-way ANOVA. (*D*) ARL4C levels from hippocampal lysates of *Rbx2* fl/fl (Ctrl) and Rbx2cKO–Emx1 (cKO) were compared at several ages by Western blotting. ARL4C accumulated in Rbx2cKO–Emx1 samples at all ages analyzed. (*E*) Coronal sections of Control (*Rbx2* fl/fl) and Rbx2cKO–Emx1 at P8 were stained with anti-ARL4C antibody and counterstained with DAPI. ARL4C is highly expressed in PNs of the CAs. (e′ and e′′) High-magnification images of the CA1 regions indicated in *E*.

Knocking down of CYTH1 or ARF6 did not rescue the PN overmigration phenotype caused by CUL5 KD, but exacerbated PN overmigration with PNs moving farther into the *sr* (Fig. 7 *D*–*F*). These results support the hypothesis, previously established in the cortex, that active ARF6 inhibits neuron migration (38). Despite the enhancement in PN displacement, no CUL5/CYTH1-KD or CUL5/ARF6-KD PNs were found in the *slm*, and, in several instances, electroporated PNs were found arrested at the boundary between *sr* and *slm*. Due to the large clustering of the CUL5/CYTH1-KD or CUL5/ARF6-KD PNs at the *sr*/*slm* boundary, we were unable to precisely determine the dendritic morphology of these neurons. However, we did not observe dendrites penetrating into the *slm* (Fig. 7 *D* and *E*). These data suggest that CRL5 participates in PN localization and apical dendrite formation by regulating ARL4C, CYTH1, and ARF6 levels.

To further understand the molecular mechanism driving PN overmigration, we individually overexpressed ARL4C, ARF6 (wild type or the constitutively activate ARF6 Q67L mutant), and FYN (wild type or the constitutively activate FYN Y528F mutant) in PNs by IUE. In any of these conditions, we did not observe PN overmigration (*SI Appendix*, Fig. S6). Next, we hypothesized that the expression of a combination of these signaling effectors would be necessary to drive PN overmigration. As shown in Fig. 7 *G* and *H*, overexpression of ARL4C, FYN, and DAB1 was sufficient to recapitulate the dendritic defects observed in shCUL5 PNs, as well as promote PN overmigration (Fig. 7 *G* and *H*). These results indicate that CRL5 regulates PN localization and the formation of a single, radially oriented apical dendrite by opposing, at least, ARL4C, FYN, and DAB1.

Given that CUL5-KD PNs did extend dendrites into the *slm*, we hypothesized that the failure to do so in CUL5/ARL4C-, CUL5/CYTH1-, and CUL5/ARF6-KD PNs would be independent of CRL5 activity, but dependent on ARL4C and ARF6 activity. To test this hypothesis, we in utero-electroporated shARL4C and shARF6 individually in the hippocampus and determined the ability of electroporated PNs to innervate the *slm*. Both ARL4C and ARF6-KD PNs were located in the *sp* and extended a single apical dendrite toward the *sr* (Fig. 7 *F* and *G*). Importantly, depletion of ARL4C or ARF6 blocked, for the most part, the ability of PNs to extend their dendrites into the *slm*. Interestingly, overexpression of the ARF6 Q67L showed the same dendritic defect (*SI Appendix*, Fig. S6*C*), indicating that tight regulation of ARF6 activation is required for PN dendritic outgrowth. Overall, these results confirm that ARL4C and ARF6 are signaling effectors involved in PN dendritic outgrowth into the *slm*.

Discussion

Our results show that CRL5 is required for PN localization and apical dendrite formation. RBX2 mutant PNs, principally those

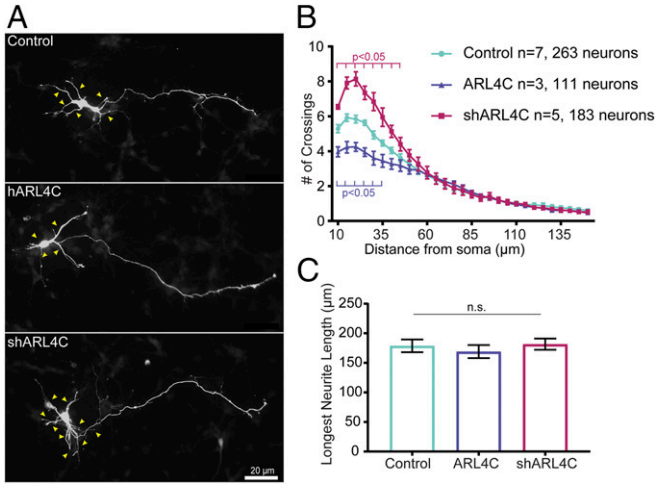

Fig. 6. ARL4C participates in dendritic development of cultured hippocampal neurons. (*A* and *B*) ARL4C negatively regulates the dendritic complexity of hippocampal neurons. E16 hippocampal primary neurons were obtained and transfected in suspension with GFP (Control) or human ARL4C/GFP (hARL4C) expression plasmids, or a shRNA against ARL4C/GFP (shARL4C) plasmids. Representative images (*A*) and Sholl analysis (*B*) from independent experiments are shown. Twenty to 50 neurons were quantified per experiment. ARL4C overexpression decreased and ARL4C knockdown increased dendritic complexity within 60 µm of soma. Yellow arrowheads indicate neurites. Mean ± SEM. Statistics, two-way ANOVA. (*C*) Length of the longest neurites were measured in each condition and no statistical differences were observe between conditions ($n = 3$). Number of neurons quantified: 125, Control; 119, ARL4C; 168, shARL4C. Mean ± SEM. Statistics, one-way ANOVA. n.s., not significant.

from the CA1 region, are ectopically displaced into the *so* and *sr/slm*. Overmigration into the *sr/slm* is a cell autonomous effect of CRL5 inactivation, as CUL5 KD by IUE does not cause displacement into the *so*. These results indicate that both cell-autonomous and compensatory or non-cell-autonomous mechanisms shape the RBX2 mutant hippocampus. CRL5 inactivation also disrupts the formation of single, radially oriented apical dendrites in PNs and promotes the formation of multiple or disrupted apical dendrites. Moreover, we uncovered ARL4C and ARL4C signaling effectors, including CYTH1, and ARF6, to be regulated by CRL5 during hippocampal development. We show that ARL4C is dynamically expressed during brain development, and its ectopic accumulation is necessary for the phenotypes observed in CRL5-depleted PNs. Finally, we show that ARL4C, CYTH1, and ARF6 participate in the outgrowth of PN apical dendrites into the *slm*.

In comparison to IUE, where the effects of acute CUL5 depletion are observed, in the RBX2 mutant, hippocampus compensatory or non–cell-autonomous mechanisms also participate in hippocampal morphogenesis. How might these mechanisms cause PN dispersion into the *so*? Recent work from Minh Nguyen and collaborators showed that reduction of Reelin expression from hippocampal interneurons in the juvenile/adult hippocampus causes PNs to disperse into the *so* (33, 39). Based on this work, we hypothesize that in the postnatal RBX2 mutant hippocampus a compensatory effect may reduce Reelin/DAB1 signaling in PNs and be responsible for the dispersion phenotype. Alternatively, RBX2 depletion in PNs may, in a non-cell-autonomous fashion, disrupt Reelin expression from interneurons triggering PN dispersion. Future work will provide formal testing of these hypotheses.

CRL5 Regulation of ARL4C Signaling and Neuron Migration. CRL5 is a crucial regulator of the proteome during CNS development. In the absence of CRL5 activity, we identified several proteins accumulated in the telencephalon, including ARL4C, CYTH1/3, ARF6, FRMD4A, FYN, and DAB1 (16, 18). Several examples of protein–protein interactions, as well as functional interconnection, have been demonstrated for these signaling effectors. ARL4C recruits all members of the cytohesin family to the plasma membrane, and, in turn, cytohesins can recruit and activate ARF6 by promoting GDP/GTP exchange (6, 40). Importantly, in Schwann cells, FYN regulates CYTH1 GEF activity toward ARF6 by phosphorylating its Tyr^{382}, a mechanism that may be present in other cytohesins (41). Finally, CYTH1 interacts with FRMD4A to activate ARF6 and regulate cell polarity, actin cytoskeleton, and membrane trafficking in epithelial and neuronal cells (42, 43). The functional interconnection among these proteins and the fact that, in the absence of CRL5 activity, all of them accumulated in the telencephalon indicates that CRL5-dependent regulation of ARL4C and ARL4C signaling effectors is critical for hippocampal development.

Different from other ARLs and ARFs, ARL4C has a spontaneous GTP binding capability that enables ARL4C to be constantly active (1, 4). In epithelial cells, ARL4C localizes preferentially at the plasma membrane, where it interacts with cytohesins, or in the nucleus (1, 6). Interestingly, our results indicate that ARL4C localizes at the plasma membrane and in punctum in the cytoplasm, whereas little ARL4C signal is detected in the nucleus. Given that no GAPs or GEFs have been described for ARL4C (2), our results that RBX2 mutant hippocampal neurons have an increased number of ARL4C-containing punctum suggest that ARL4C activity may be regulated by CRL5-dependent turnover or by sequestering ARL4C in cytoplasmic vesicles and away from the plasma membrane.

ARL4C is necessary for PN overmigration upon CRL5 inactivation and together with FYN and DAB1 sufficient to trigger it. FYN and DAB1 participate in a positive-feedback loop, resulting in activation of both signaling effectors (44, 45). Future work should determine whether accumulation of these three proteins is necessary to cause PN migration or, alternatively, ARL4C only requires active FYN or DAB1 to elicit neuron migration. In the neocortex, ARF6 inactivation (i.e., ARF6–GDP) is required for cortical neuron migration (12, 38). Thus, we propose a model where accumulation of ARL4C, FYN, and DAB1 promotes PN migration, and, at the same time, ARL4C recruits CYTH1 to the plasma membrane, activating ARF6, which partially opposes overmigration. Then, depletion of CYTH1 or ARF6 enhances PN overmigration caused by CUL5 KD.

CRL5 and ARL4C Signaling Participates on PN Dendritogenesis. The "V-shape" dendritic phenotype described in RBX2 mutant and CUL5 KD PNs demonstrates the cell-autonomous role of CRL5 in PN apical dendrite formation. V-shaped dendrites have been described in granule cells of the mouse hippocampus in response to stress, inflammation, or in neurodegenerative models, including models of Alzheimer's disease (AD) and frontotemporal dementia, as well as in the brains of AD patients (46–48). Considering that CUL5 KD acts cell-autonomously, it is unlikely that stress or inflammation may be responsible for the phenotypes observed upon CRL5 inactivation. Interestingly, Tau secretion promotes V-shaped dendrites in hippocampal granule cells (49). Importantly, CYTH1 and FRMD4A modulates TAU secretion (42), and CYTH1, FRMD4A, and TAU accumulate in the RBX2 mutant telencephalons (Dataset S1). Moreover, ARL4C and FYN are necessary to bind and activate CYTH1, and overexpression of ARL4C, FYN, and DAB1 is sufficient to promote the V-shape dendritic phenotype. This suggest that, in the absence of CRL5, TAU secretion may be enhanced, stimulating the formation of V-shaped apical dendrites.

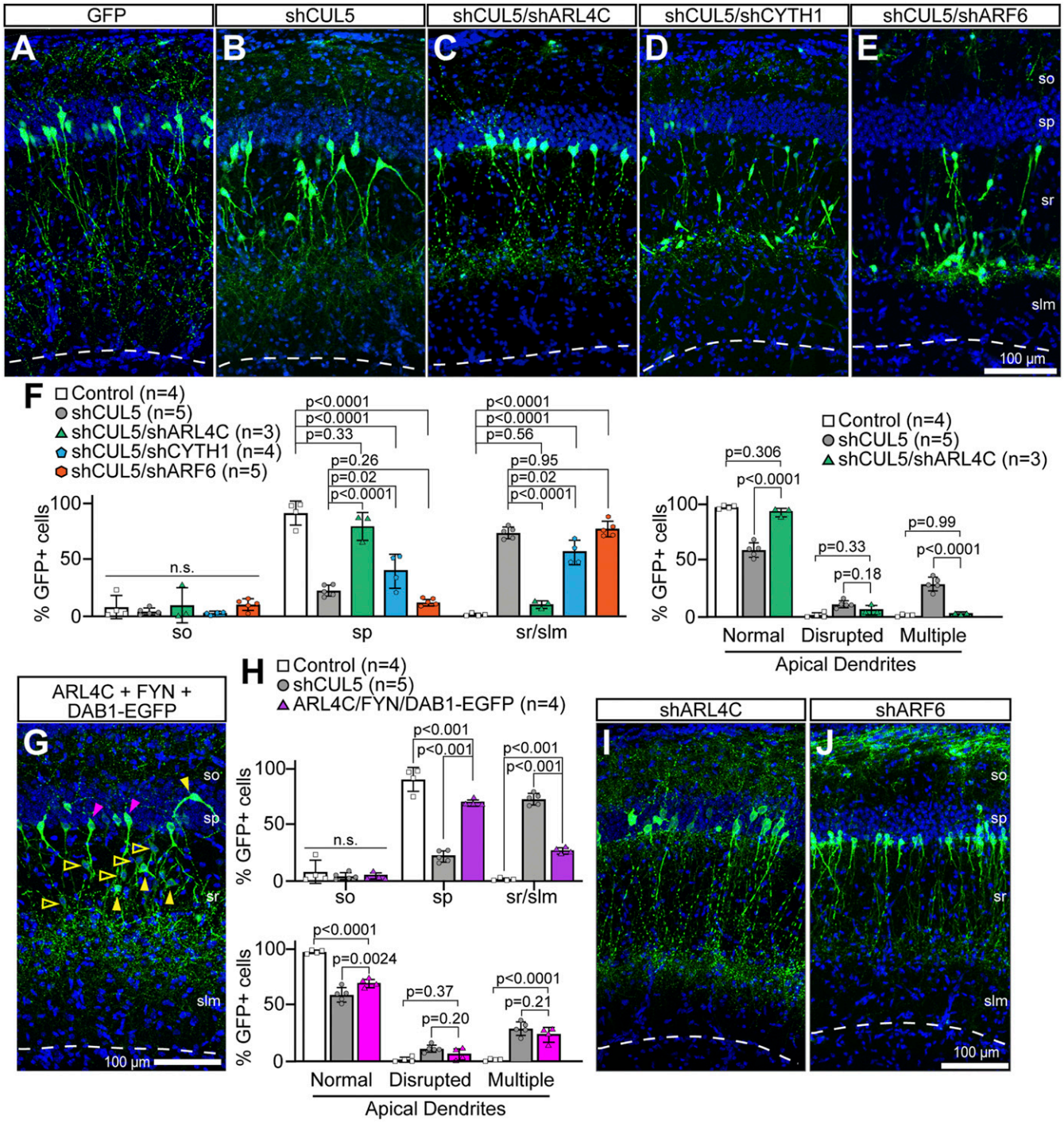

Fig. 7. ARL4C and ARF6 have opposite effects on CRL5-dependent PN overmigration, but the same effects on PN dendrite extension into the *slm*. (*A*–*E*) Representative images of hippocampus electroporated at E15 and collected at P10 showing control (GFP) (*A*), CUL5 KD (shCUL5) (*B*), double CUL5/ARL4C KD (shCUL5/shARL4C) (*C*), double CUL5/CYTH1 KD (shCUL5/shCYTH1) (*D*), and double CUL5/ARF6 KD (shCUL5/shARF6) (*E*) transfected PNs. Whereas ARL4C KD rescue the PN overmigration phenotype caused by CUL5 KD, CYTH1 and ARF6 KD exacerbated it. CUL5/ARL4C-, CUL5/ARF6-, and CUL5/CYTH1-KD PNs fail to extend their apical dendrites into the *slm* in comparison to control or CUL5-KD PNs. The striped lines represent the hippocampal fissure. (*F*) Quantification of the percentage number of GFP + cells in each strata (*Left*) and percentage of GFP + cells with normal, disrupted, or multiple apical dendrites (*Right*). Mean ± SD. Statistics, two-way ANOVA with Tukey's multiple-comparison test. (*G*) Overexpression of ARL4C, CYTH1, and DAB1–EGFP by IUE is sufficient to mimic CUL5 KD phenotypes (*B*). Pink arrowheads indicate PNs with correct position. Yellow solid arrowheads indicate PNs with abnormal apical dendrites. Yellow hollow arrowheads indicate overmigrated PNs. The striped lines represent the hippocampal fissure. (*H*) Quantification of the percentage number of GFP+ cells in each strata (*Upper*) and percentage of GFP + cells with normal, disrupted, or multiple apical dendrites (*Lower*). Mean ± SD. Statistics, two-way ANOVA with Tukey's multiple comparison test. (*I* and *J*) Single ARL4C (shARL4C) (*I*) or ARF6 (shARF6) (*J*) KD constructs were cotransfected with GFP by IUE in E15 hippocampi and brains were collected at P10. In both conditions, PNs migrated normally and had a single radially oriented apical dendrite, but failed to extend their dendrites into the *slm*. The striped lines represent the hippocampal fissure.

Our data also indicate that ARL4C, CYTH1, and ARF6 participate in PN dendritogenesis in vitro and in vivo. In vivo, all three signaling effectors regulate PN dendritic outgrowth into the *slm*. Interestingly, endogenous ARL4C expression peaks during PN dendritogenesis at early postnatal stages. We hypothesize that higher ARL4C levels are necessary to activate ARL4C signaling, triggering the dendritic outgrowth into the *slm*. However, ARL4C signaling must be tightly controlled, as excessive ARF6 activation (i.e., ARF6–GTP) is also deleterious for the dendritic outgrowth into the *slm*.

Materials and Methods

Animals. All animals were used with approval from the University of California, Davis Institutional Animal Care and Use Committees and housed and cared for in accordance with the guidelines provided by the National Institutes of Health. *Rbx2* floxed (*Rbx2* fl/fl), *Rbx2 fl/fl; Nestin–Cre/+* (Rbx2cKO–Nes) mice were obtained as described (18). To generate *Rbx2 fl/fl; Emx1–Cre/+* (Rbx2cKO–Emx1) mice, *Rbx2 fl/fl* were crossed with *Emx1–Cre/+* mice (31). Rbx2cKO–Emx1 mice were viable and fertile and survive until adulthood without any evidence of hydrocephalus. *socs7* heterozygous and knockout mice were obtained as described (16). CD-1 mice were used for IUE experiments and Sholl analysis (Charles River). Females were mated, and the morning a vaginal plug was observed was considered E0.5. In utero microinjection and electroporation were performed as described (18).

Constructs. The pSG5–hARL4C construct was a generous gift from Fang-Jen Lee, National Taiwan University, Taiwan (4). pcDNA3–HA–ARF6 and pcDNA3–HA–ARF6 Q67L were a gift from Thomas Roberts, Harvard Medical School, Boston, MA [Addgene plasmid nos. 10834 and 10835, respectively (50)]. For our experiments, hARL4C and both HA-ARF6s were subclone into a pCAG vector (18). The pGEX-4T-2/hGGA3(GAT) plasmid was a gift from Kazuhisa Nakayama, Kyoto University, Kyoto, Japan [Addgene plasmid catalog no. 79436 (51)]. shRNAs were cloned into pSUPER (Oligoengine), according to manufacturer recommendations [shARL4C, 5′-AGTTCACACAGAAACCCTGGG-3′; shARF6, 5′-AGCTGCACCGCATTATCAA-3′ (52); shCYTH1, 5′-AAGATTGACCGGATGATGGAG-3′; shFYN, 5′-ACAGGTTGCTGCAGGAATG-3′] or into pMX-puro [shCUL5, 5′-GCTGCAGACTGAATTAGTAG-3′ (20)]. For shRNA efficiency, see *SI Appendix*, Fig. S7.

Histology and Immunohistochemistry. Two-week-old and older mice were anesthetized and transcardially perfused with phosphate-buffered saline (PBS) followed by 3.7% formalin/PBS using a peristaltic pump. Perfused fixed brains were collected and postfixed at 4 °C overnight in the same solution. Tissues were cryoprotected with 30% sucrose/PBS solution. Next, brains were embedded in Optimum Cutting Temperature (OCT) compound (Tissue-Tek) and quickly frozen by using dry-ice. OCT-embedded brain blocks were cryosectioned on a coronal plane (30 μm). Immunostainings were performed in free-floating sections with agitation. Sections were blocked with PBS, 0.5% Triton X-100, and 5% milk or 10% normal donkey serum for 1 h at room temperature. Blocking solution, but reducing Triton X-100 concentration to 0.3%, was used for primary antibody incubation (overnight, 4 °C). The following primary antibodies were used for immunohistochemistry: anti-CTIP2 (1:400; Abcam catalog no. ab18465), anti-CUX1 (1:50; Santa Cruz Antibodies catalog no. sc-13024, discontinued), anti-DKK3 (1:200; SinoBiological catalog no. 50247-RP02), anti-DAB1 (1:100; Sigma-Aldrich catalog no. HPA052033), anti-ARL4C (1:100; Proteintech catalog no. 10202-1), anti-MAP2 (1:200; Abcam catalog no. 5392), and anti-GFP (1:200; Life Technologies catalog no. A11122). After primary antibody incubation, free-floating sections were washed three times in PBS/0.1% Triton X-100 (10 min each). Species-specific Alexa Fluor 488-, 568-, and/or 647-conjugated immunoglobulin G (IgG) (1:200; Life Technologies) were used in blocking solution, but reducing Triton X-100 concentration to 0.3% (90 min, room temperature). DAPI (Sigma-Aldrich) was used for nuclear staining. Images were taken in a Fluoview FV3000 confocal microscope (Olympus) or Axio Imager.M2 with Apotome.2 microscope system (Zeiss). All images were assembled by using Photoshop and Illustrator (Adobe).

Golgi-Cox Stainings. Golgi-Cox stainings were performed on freshly dissected P15 *Rbx2* fl/fl and Rbx2cKO-Nes brains by using the FD Rapid GolgiStain Kit, according to the manufacturer protocol (FD NeuroTechnologies catalog no. PK401A).

Primary Cultures. E17.5 hippocampal neurons were dissociated by using papain following manufacturer instructions (Worthington Papain Dissociation Systems catalog no. LK003150). A concentration of 0.5 M cells was plated on poly-D-lysine (0.05 μg/μL)-coated glass coverslips. Neurons were transfected in suspension immediately following dissociation by using Lipofectamine 2000 (ThermoFisher catalog no. 11668019) following manufacturer protocol. Neurons were cultured in Neurobasal medium containing 1× penicillin/streptomycin, 1× GlutaMAX, 30 mM D-glucose, and B27 supplement. Medium was changed every 2 d, and neurons were fixed at indicated time points by using 3.7% formalin/PBS for 15 min at 4 °C.

Sholl Analyses/Neurite Measurements. Hippocampal primary neurons were transfected in suspension on the day of isolation with 0.2 μg of pCAG–GFP, 0.2 μg of pCAG–GFP, and 1 μg of pCAG–hARL4C, or 0.2 μg of pCAG–GFP and 1 μg of pSUPER–shARL4C as indicated. Neurons were fixed at 2 DIV and stained against GFP. GFP+ neurons were imaged in a Zeiss epifluorescence microscope. Neurite complexity in each condition was measured by placing a grid of concentric circles, with 5-μm radius increment, around the neuron cell body and counting the number of neurites crossing each circle. The longest neurite length was measured by using ImageJ plugin Simple Neurite Tracer.

RNA-Seq. RNA from *Rbx2* fl/fl ($n = 3$) and Rbx2cKO–Nes ($n = 3$) P1 telencephalons was extracted by using TRIzol (Invitrogen). Strand-specific and barcode-indexed RNA-seq libraries were generated from 1 μg of total RNA each after poly-A enrichment by using the Kapa Stranded mRNA-seq kit (Kapa Biosystems) following manufacturer instructions. Libraries were analyzed with a Bioanalyzer 2100 instrument (Agilent), quantified by fluorometry on a Qubit instrument (Life Technologies), and pooled in equimolar ratios. The pool was quantified by qPCR with a Kapa Library Quant kit (Kapa Biosystems) and sequenced on one high-output flow cell of an Illumina NextSeq 500 (Illumina) with paired-end 40-bp reads.

RNA Analyses. Total RNA from CD-1 wild-type telencephalon was isolated by using TRIzol. The iSCRIPT system (Bio-Rad) was used for complementary DNA reverse-transcription. *Arl4c* or *β-Actin* transcripts were quantified by real-time PCR using gene-specific primers and iTaq Universal SYBR Green Supermix (Bio-Rad). ΔCt (*β-Actin* Ct – *Arl4c*-Ct) values were used to compare the ARL4C expression at the different time points.

Primers used were: *β-Actin*, 5′-CTAAGGCCAACCGTGAAAAG-3′ and 5′-ACCAGAGGCATACAGGGACA-3′; and *Arl4c*, 5′-AGTCTCTGCACATCGTTATGC-3′ and 5′-GGTGTTGAAGCCGATAGTGGG-3′.

TMT MS. P0 *Rbx2* fl/fl ($n = 4$) and Rbx2cKO–Nes ($n = 3$) pups were intracardially perfused with a solution of PBS and protease and phosphatase inhibitors (1 mM phenylmethylsulfonyl fluoride [PMSF], 10 μg/mL Aprotinin, 10 μg/mL Leupeptin, 10 mM NaF, and 1 mM Na_3VO_4). Telencephalons from these animals were quickly dissected and snap-frozen. Samples were labeled by using the isobaric TMT method and analyzed and quantified by MS. Briefly, proteins were lysed and processed for sequential digestion by using LysC and trypsin. Peptides from each embryo were labeled with the TMT reagents, such the reporter ions at *m/z* 126, 127N, 127C, and 128N for control samples (i.e., *Rbx2* fl/fl) and 128C, 129N, and 131 for RBX2 mutant samples would be generated in the tandem spectrometry. Liquid chromatography, MS3 tandem MS, and data analysis were carried out as described (53, 54).

Western Blot Analyses. Total protein extracts from dissected cortices or hippocampi were prepared by homogenizing tissues in an appropriate volume of ice-cold lysis buffer (50 mM Hepes, pH7.5, 150 mM NaCl, 1.5 mM $MgCl_2$, 1 mM ethylene glycol tetraacetic acid, 10% glycerol, and 1% Triton X-100) using a Pellet Pestle Motor tool (Kontes). Protease and phosphatase inhibitors (1 mM PMSF, 10 μg/mL Aprotinin, 10 μg/mL Leupeptin, 10 mM NaF, and 1 mM Na_3VO_4) were added to the lysis buffer just prior to homogenization. The homogenate was cold-centrifuged for 15 min at 14,000 rpm. A total of 20 μL of cleared supernatant was denatured at 95 °C for 10 min in sample buffer (10 mM Tris, pH 6.5, 150 mM β-mercaptoethanol, 0.5% sodium dodecyl sulfate (SDS), 5% glycerol, and 0.0125% bromophenol blue) and loaded into a (SDS)-polyacrylamide gel, to finally be transferred to a 0.2-μm nitrocellulose membrane (Bio-Rad) using standard methods. Membranes were blocked for 1 h with blocking solution (Tris-buffered saline with 0.1% Tween-20 [TBS-T], 5% nonfat milk powder, or 5% bovine serum albumin), washed with TBS-T and incubated overnight with primary antibodies (anti-Actin 1:10,000; Santa Cruz Biotechnology catalog no. sc1616; anti-DAB1 1:2,000, Sigma-Aldrich catalog no. HPA052033; anti-FYN 1:1,000, Santa Cruz Biotechnology catalog no. sc-16; anti-Tuj1, 1:20,000 BioLegend catalog no. 801201; anti-HA, 1:10,000 BioLegend catalog no. 901501; anti-ARL4C 1:1,000, Proteintech catalog no. 10202-1; and anti-CYTH1 1:1,000, Fisher Scientifics catalog no. MA1060). Specific horseradish peroxidase-conjugated secondary antibodies were incubated for 45 min at room temperature

in blocking solution. Proteins were identified by using SuperSignal West Pico enhanced chemiluminescence (ECL) substrate (ThermoFisher ScientificMA) or ProSignal Femto ECL reagent (Genesee Scientific) by exposing to X-ray films. Films were scanned on an Epson perfection V600 photo scanner and converted to 16-bit images for band-densitometry quantification using FIJI software (ImageJ2, Version 1.51t, NIH). Protein abundancy was calculated upon band densitometry analysis compared to littermate controls, and results were normalized by using the detection of Actin or Tuj1 as a loading control. All images were assembled by using Adobe Photoshop and Illustrator.

Coimmunoprecipitation Assay. The hippocampal regions of control (*Rbx2* fl/fl) or Rbx2cKO-Emx1 mice were carefully dissected, lysed, mixed with 3 μL of anti-CYTH1 antibody, and incubated at 4 °C for 2 h. Next, Protein A/G-Agarose beads were used to immunoprecipitate CYTH1, and Western blotting was used to detect coimmunoprecipitated ARF6.

GGA3-GST Pull down Assay. The hippocampal regions of control (*Rbx2* fl/fl) or Rbx2cKO–Emx1 mice were carefully dissected, lysed and pulled down by using the GST fusion protein containing GGA3 ARF-binding domain (107 to 286 aa) as described (36).

Hippocampal Quantifications and Statistical Methods. For all in vivo datasets, biological replicates were obtained from at least two different litters or IUEs. Specific number of biological replicates (Ns) are specified in each figure/figure legend. For hippocampal size and DKK3+ cell quantification, we quantified both hippocampal hemispheres of three sections containing the dorsal hippocampus in which the habenula was visible. For IUEs, all detected GFP+ cell bodies in the CA1/CA2 regions were quantified for at least three electroporated sections in each brain; for dendrite quantifications, only those cells where a clear apical dendrite(s) was observed were used for our quantifications. For in vitro ARL4C puncta analysis, five neurons were quantified per embryo and compared to wild-type littermate controls. Unless indicated, histograms represent the mean ± the SEM. Specific statistical tests used in each case are indicated in figure legends. All statistical analyses and plot generation were performed by using Prism 8 (GraphPad).

Data Availability. The sequences reported in this paper have been deposited in Gene Expression Omnibus (GEO) database, https://www.ncbi.nlm.nih.gov/geo/ (accession no. GSE155379). All study data are included in the article and *SI Appendix*.

ACKNOWLEDGMENTS. We thank Dr. Fang-Jen Lee and Dr. Thomas Roberts for their generosity sharing reagents; Dr. Jonathan A. Cooper for critical reading of the manuscript; Dr. Monica Britton for her help analyzing RNA-seq data; and Ysidra Camarena for technical assistance. We particularly thank Dr. Ryan C. Kunz and the Thermo Fisher Scientific Center for Multiplexed Proteomics service core (Harvard University) for running our TMT-MS experiment. This work was supported by NIH Grants R01 NS109176 (to S.S.) and R21 NS101450 (to S.S. and A.L.T.). We also benefited from the use of the National Eye Institute Core Facilities (supported by NIH Grant P30 EY012576) and the Health Sciences District Advanced Imaging Facility (University of California, Davis).

1. S. Matsumoto, S. Fujii, A. Kikuchi, Arl4c is a key regulator of tubulogenesis and tumourigenesis as a target gene of Wnt-β-catenin and growth factor-Ras signalling. *J. Biochem.* **161**, 27–35 (2017).
2. E. Sztul *et al*., ARF GTPases and their GEFs and GAPs: Concepts and challenges. *Mol. Biol. Cell* **30**, 1249–1271 (2019).
3. S. Jacobs *et al*., ADP-ribosylation factor (ARF)-like 4, 6, and 7 represent a subgroup of the ARF family characterization by rapid nucleotide exchange and a nuclear localization signal. *FEBS Lett.* **456**, 384–388 (1999).
4. T. S. Chiang, H. F. Wu, F. S. Lee, ADP-ribosylation factor-like 4C binding to filamin-A modulates filopodium formation and cell migration. *Mol. Biol. Cell* **28**, 3013–3028 (2017).
5. S. Matsumoto *et al*., A combination of Wnt and growth factor signaling induces Arl4c expression to form epithelial tubular structures. *EMBO J.* **33**, 702–718 (2014).
6. I. Hofmann, A. Thompson, C. M. Sanderson, S. Munro, The Arl4 family of small G proteins can recruit the cytohesin Arf6 exchange factors to the plasma membrane. *Curr. Biol.* **17**, 711–716 (2007).
7. C. Albertinazzi, L. Za, S. Paris, I. de Curtis, ADP-ribosylation factor 6 and a functional PIX/p95-APP1 complex are required for Rac1B-mediated neurite outgrowth. *Mol. Biol. Cell* **14**, 1295–1307 (2003).
8. D. J. Hernández-Deviez, M. G. Roth, J. E. Casanova, J. M. Wilson, ARNO and ARF6 regulate axonal elongation and branching through downstream activation of phosphatidylinositol 4-phosphate 5-kinase alpha. *Mol. Biol. Cell* **15**, 111–120 (2004).
9. R. Eva *et al*., ARF6 directs axon transport and traffic of integrins and regulates axon growth in adult DRG neurons. *J. Neurosci.* **32**, 10352–10364 (2012).
10. Y. Miura *et al*., ACAP3 regulates neurite outgrowth through its GAP activity specific to Arf6 in mouse hippocampal neurons. *Biochem. J.* **473**, 2591–2602 (2016).
11. D. N. Arvanitis *et al*., Ephrin B1 maintains apical adhesion of neural progenitors. *Development* **140**, 2082–2092 (2013).
12. A. Falace *et al*., TBC1D24 regulates neuronal migration and maturation through modulation of the ARF6-dependent pathway. *Proc. Natl. Acad. Sci. U.S.A.* **111**, 2337–2342 (2014).
13. M. H. Glickman, A. Ciechanover, The ubiquitin-proteasome proteolytic pathway: Destruction for the sake of construction. *Physiol. Rev.* **82**, 373–428 (2002).
14. M. D. Petroski, R. J. Deshaies, Function and regulation of cullin-RING ubiquitin ligases. *Nat. Rev. Mol. Cell Biol.* **6**, 9–20 (2005).
15. F. Okumura, A. Joo-Okumura, K. Nakatsukasa, T. Kamura, The role of cullin 5-containing ubiquitin ligases. *Cell Div.* **11**, 1 (2016).
16. C. L. Fairchild *et al*., RBX2 maintains final retinal cell position in a DAB1-dependent and -independent fashion. *Development* **145**, dev155283 (2018).
17. K. Hino, S. Simó, J. A. Cooper, Comparative analysis of cul5 and rbx2 expression in the developing and adult murine brain and their essentiality during mouse embryogenesis. *Dev. Dyn.* **247**, 1227–1236 (2018).
18. S. Simó, J. A. Cooper, Rbx2 regulates neuronal migration through different cullin 5-RING ligase adaptors. *Dev. Cell* **27**, 399–411 (2013).
19. M. S. Cembrowski, L. Wang, K. Sugino, B. C. Shields, N. Spruston, Hipposeq: A comprehensive RNA-seq database of gene expression in hippocampal principal neurons. *eLife* **5**, e14997 (2016).
20. L. Feng, N. S. Allen, S. Simo, J. A. Cooper, Cullin 5 regulates Dab1 protein levels and neuron positioning during cortical development. *Genes Dev.* **21**, 2717–2730 (2007).
21. S. Simó, Y. Jossin, J. A. Cooper, Cullin 5 regulates cortical layering by modulating the speed and duration of Dab1-dependent neuronal migration. *J. Neurosci.* **30**, 5668–5676 (2010).
22. K. Sekine, K. Kubo, K. Nakajima, How does Reelin control neuronal migration and layer formation in the developing mammalian neocortex? *Neurosci. Res.* **86**, 50–58 (2014).
23. C. R. Wasser, J. Herz, Reelin: Neurodevelopmental architect and homeostatic regulator of excitatory synapses. *J. Biol. Chem.* **292**, 1330–1338 (2017).
24. L. Pujadas *et al*., Reelin regulates postnatal neurogenesis and enhances spine hypertrophy and long-term potentiation. *J. Neurosci.* **30**, 4636–4649 (2010).
25. R. Knox, X. Jiang, Fyn in neurodevelopment and ischemic brain injury. *Dev. Neurosci.* **37**, 311–320 (2015).
26. G. Kuo, L. Arnaud, P. Kronstad-O'Brien, J. A. Cooper, Absence of Fyn and Src causes a reeler-like phenotype. *J. Neurosci.* **25**, 8578–8586 (2005).
27. S. G. Grant *et al*., Impaired long-term potentiation, spatial learning, and hippocampal development in fyn mutant mice. *Science* **258**, 1903–1910 (1992).
28. P. Andersen, *The Hippocampus Book* (Oxford University Press, Oxford, UK, 2007), p. 832.
29. R. Khalaf-Nazzal, F. Francis, Hippocampal development—Old and new findings. *Neuroscience* **248**, 225–242 (2013).
30. J. Altman, S. A. Bayer, Migration and distribution of two populations of hippocampal granule cell precursors during the perinatal and postnatal periods. *J. Comp. Neurol.* **301**, 365–381 (1990).
31. H. Guo *et al*., Specificity and efficiency of Cre-mediated recombination in Emx1-Cre knock-in mice. *Biochem. Biophys. Res. Commun.* **273**, 661–665 (2000).
32. D. B. Diep, N. Hoen, M. Backman, O. Machon, S. Krauss, Characterisation of the Wnt antagonists and their response to conditionally activated Wnt signalling in the developing mouse forebrain. *Brain Res. Dev. Brain Res.* **153**, 261–270 (2004).
33. Y. Jiang *et al*., Ndel1 and Reelin maintain postnatal CA1 hippocampus integrity. *J. Neurosci.* **36**, 6538–6552 (2016).
34. S. Niu, A. Renfro, C. C. Quattrocchi, M. Sheldon, G. D'Arcangelo, Reelin promotes hippocampal dendrite development through the VLDLR/ApoER2-Dab1 pathway. *Neuron* **41**, 71–84 (2004).
35. A. Thompson *et al*., Tandem mass tags: A novel quantification strategy for comparative analysis of complex protein mixtures by MS/MS. *Anal. Chem.* **75**, 1895–1904 (2003).
36. R. Charles, M. Bourmoum, S. Campbell, A. Claing, Methods to investigate the β-Arrestin-mediated control of ARF6 activation to regulate trafficking and actin cytoskeleton remodeling. *Methods Mol. Biol.* **1957**, 159–168 (2019).
37. E. Nakahira, S. Yuasa, Neuronal generation, migration, and differentiation in the mouse hippocampal primoridium as revealed by enhanced green fluorescent protein gene transfer by means of in utero electroporation. *J. Comp. Neurol.* **483**, 329–340 (2005).
38. Y. Hara *et al*., ADP ribosylation factor 6 regulates neuronal migration in the developing cerebral cortex through FIP3/Arfophilin-1-dependent endosomal trafficking of N-cadherin. *eNeuro* **3**, ENEURO.0148-16.2016 (2016).
39. I. Kiroski *et al*., Reelin improves cognition and extends the lifespan of mutant Ndel1 mice with postnatal CA1 Hippocampus deterioration. *Cereb. Cortex* **30**, 4964–4978 (2020).
40. C. D. H. Ratcliffe *et al*., HGF-induced migration depends on the PI(3,4,5)P_3-binding microexon-spliced variant of the Arf6 exchange factor cytohesin-1. *J. Cell Biol.* **218**, 285–298 (2019).
41. J. Yamauchi *et al*., Phosphorylation of cytohesin-1 by Fyn is required for initiation of myelination and the extent of myelination during development. *Sci. Signal.* **5**, ra69 (2012).
42. X. Yan *et al*., FRMD4A-cytohesin signaling modulates the cellular release of tau. *J. Cell Sci.* **129**, 2003–2015 (2016).

43. J. Ikenouchi, M. Umeda, FRMD4A regulates epithelial polarity by connecting Arf6 activation with the PAR complex. *Proc. Natl. Acad. Sci. U.S.A.* **107**, 748–753 (2010).
44. L. Arnaud, B. A. Ballif, E. Förster, J. A. Cooper, Fyn tyrosine kinase is a critical regulator of disabled-1 during brain development. *Curr. Biol.* **13**, 9–17 (2003).
45. H. H. Bock, J. Herz, Reelin activates SRC family tyrosine kinases in neurons. *Curr. Biol.* **13**, 18–26 (2003).
46. M. Llorens-Martín, A. Rábano, J. Ávila, The ever-changing morphology of hippocampal granule neurons in physiology and pathology. *Front. Neurosci.* **9**, 526 (2016).
47. J. Terreros-Roncal *et al*., Activity-dependent reconnection of adult-born dentate granule cells in a mouse model of frontotemporal dementia. *J. Neurosci.* **39**, 5794–5815 (2019).
48. M. Llorens-Martín *et al*., GSK-3β overexpression causes reversible alterations on postsynaptic densities and dendritic morphology of hippocampal granule neurons in vivo. *Mol. Psychiatry* **18**, 451–460 (2013).
49. M. Bolós *et al*., Soluble Tau has devastating effects on the structural plasticity of hippocampal granule neurons. *Transl. Psychiatry* **7**, 1267 (2017).
50. C. Furman, S. M. Short, R. R. Subramanian, B. R. Zetter, T. M. Roberts, DEF-1/ASAP1 is a GTPase-activating protein (GAP) for ARF1 that enhances cell motility through a GAP-dependent mechanism. *J. Biol. Chem.* **277**, 7962–7969 (2002).
51. H. Takatsu, K. Yoshino, K. Toda, K. Nakayama, GGA proteins associate with Golgi membranes through interaction between their GGAH domains and ADP-ribosylation factors. *Biochem. J.* **365**, 369–378 (2002).
52. Y. Kim *et al*., ADP-ribosylation factor 6 (ARF6) bidirectionally regulates dendritic spine formation depending on neuronal maturation and activity. *J. Biol. Chem.* **290**, 7323–7335 (2015).
53. G. C. McAlister *et al*., MultiNotch MS3 enables accurate, sensitive, and multiplexed detection of differential expression across cancer cell line proteomes. *Anal. Chem.* **86**, 7150–7158 (2014).
54. L. Ting, R. Rad, S. P. Gygi, W. Haas, MS3 eliminates ratio distortion in isobaric multiplexed quantitative proteomics. *Nat. Methods* **8**, 937–940 (2011).